J Mater Sci (2007) 42:9954–9965
DOI 10.1007/s10853-007-2061-4

Formation and retention of local melted films in AZ91 friction stir spot welds

Peter Su · Adrian Gerlich · Motomichi Yamamoto · Thomas H. North

Received: 8 August 2006 / Accepted: 26 July 2007 / Published online: 6 September 2007

Abstract The formation of local melted films during friction stir spot welding of as-cast AZ91D and thixomolded AZ91 material is investigated. The average temperatures close to the tip of the rotating pin vary from 438 to 454 °C during the dwell period in friction stir spot welding. These measured temperature values are higher than the melting temperature of α-Mg + $Mg_{17}Al_{12}$ eutectic (437 °C). It is suggested that the temperature in the stir zone during the dwell period is determined by the relative proportions of α-Mg and (α-Mg + $Mg_{17}Al_{12}$) eutectic material, which are incorporated during friction stir spot welding. Based on the stir zone temperature measurements and a detailed examination of material located at the root of the pin thread it is suggested that material is moved downwards via the pin thread and into the stir zone during the dwell period in friction stir spot welding. Evidence of local melted film formation is observed in the stir zone of AZ91 spot welds. It is suggested that melted films are retained since their dissolution rate is much slower in the high temperature stir zone than it is when melted films is formed in the stir zone during Al 7075-T6 friction stir spot welding. The spontaneous melting temperature, solute diffusion rate and the thermodynamic driving force for droplet dissolution are much higher during Al 7075-T6 friction stir spot welding.

P. Su · A. Gerlich (✉) · M. Yamamoto · T. H. North
Department of Materials Science & Engineering, University of Toronto, 184 College St., Room 140, Toronto, ON, Canada M5S 3E4
e-mail: gerlich@ecf.utoronto.ca

Introduction

Friction stir spot welding is a variant of friction stir seam welding where the welded joint is produced at a single location. The power density is very high (around 10^{10} W/m^3 [1, 2]), the heating rate during tool penetration stage in spot welding ranges from approximately 200 to 400 °C/s [3] and the stir zone temperature approaches the solidus temperature of the Al-alloy or Mg-alloy sheet material that is being welded [4–7]. The stir zone has a fine-grained, dynamically recrystallized stir zone microstructure while the mechanical properties of completed spot welds are similar to those found during resistance spot welding [8]. This readily explains why there is considerable interest in evaluating friction stir spot welding as a possible alternative during the fabrication of automotive components.

The welding cycle can be extended during friction stir spot welding by applying a 4-s long-dwell period once the rotating pin is fully-penetrated into the contacting sheets. During the dwell period, the tool rotational speed remains constant and the axial force and torque decrease while the rotating tool penetrates about 350 μm into the surface of the upper sheet due to machine compliance [3]. It has been recently confirmed that the dimensions of the stir zone formed adjacent to the periphery of the rotating pin are significantly increased during the dwell period in spot welding, since the material from the locations beneath the tool shoulder and the bottom of the rotating pin is incorporated at the top of the rotating pin and is transferred downwards via the pin thread [9, 10].

Since the microstructure of as-cast AZ91D comprises cored α-Mg with a divorced eutectic of (α-Mg + $Mg_{17}Al_{12}$) at interdendritic boundaries and thixomolded AZ91 comprises primary α-Mg islands in a matrix of (α-Mg + $Mg_{17}Al_{12}$) eutectic, it would be expected that the

temperature might vary during the dwell period in spot welding depending on relative proportions of α-Mg and (α-Mg + $Mg_{17}Al_{12}$) eutectic, which are incorporated into the stir zone. With this in mind, the present article investigates the process of material incorporation and the resulting temperature changes produced during the dwell period in AZ91 friction stir spot welding.

Incorporated (α-Mg + $Mg_{17}Al_{12}$) eutectic material will melt spontaneously when the stir zone temperature during AZ91 spot welding is ≥437 °C. Once formed, the droplets of melted eutectic will begin to dissolve as Mg and Al diffuse into the surrounding matrix. The dissolution kinetics of liquid droplets at temperatures close to the eutectic temperature has been examined during upquenching of Al–Cu and Al–Mg–Zn alloy sections [11–13] and during the dwell period in Al 7075-T6 friction stir spot welding [3]. For example, Gerlich et al. [3] reported that the dissolution time for melted eutectic droplets within the stir zone during Al 7075-T6 spot welding ranged from 0.06 to 3 s depending on their size and shape. Bearing this in mind, the likelihood of finding metallographic evidence confirming melted eutectic formation within the stir zone of AZ91 spot welds will be determined by the supply of eutectic material during the dwell period, the kinetics of dissolution of melted eutectic droplets in the high temperature stir zone and particle dissolution as the spot weld cools to room temperature following tool retraction. In addition, the dissolution kinetics of droplets of melted eutectic will be determined by their dimensions, the time available for dissolution, the solute diffusion rate and the thermodynamic driving force for dissolution. With this in mind, the present article investigates the formation and retention local melted films in the stir zones of AZ91 friction stir spot welds.

Experimental procedure

All friction stir spot welding trials were carried out using 6.3 mm thick × 30 mm diameter sections of as-cast AZ91D and a thixomolded semi-solid AZ91 extrusion. The microstructure of the AZ91D sections comprised cored α-Mg grains and a divorced eutectic of (α-Mg + $Mg_{17}Al_{12}$) at interdendritic boundaries. In thixmolded AZ91 sections, the microstructure comprised islands of primary α-Mg embedded in matrix of α-Mg plus (α-Mg + $Mg_{17}Al_{12}$) eutectic, see Fig. 1a and b. Both base materials had a nominal composition of Mg, 9 wt.% Al, 0.7 wt.% Zn.

It must be stressed at the outset that the objective in this particular study involved determining the process of material incorporation and the resulting temperature changes during the dwell period in AZ91 friction stir spot welding. For this reason no attempt was made to homogenize the as-cast AZ91 sections prior to spot welding. Also, the microstructures of the thixomolded AZ91 sections differ from those generally observed in sheet material since the primary α-Mg islands are not concentrated toward the mid-thickness location and are instead observed through the whole section thickness.

The spot welding equipment used in the present study had a rotational speed capability up to 3,000 rpm while a servomotor provided axial loads up to 12 kN. The friction stir spot welding tool was machined from H13 tool steel, heat-treated to a hardness of 46–48 HRc, which minimized tool wear during spot welding. The tool used in the present study had a shoulder diameter of 10 mm, a pin diameter of 4 mm, a pin length of 2.2 mm and a M4 metric thread geometry as shown in Fig. 2. Plunge rates up to 25 mm/s were selectable during spot welding, with the penetration depth being attained with an accuracy of ±0.1 mm. During friction stir spot welding the tool penetration (displacement) was measured using a linear transducer with an accuracy of ±0.01 mm, while the axial load and torque were measured using a JR3 six-axis load cell, which was

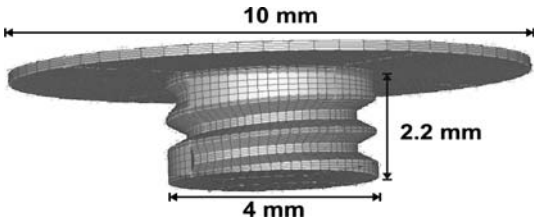

Fig. 2 Tool geometry used during friction stir spot welding

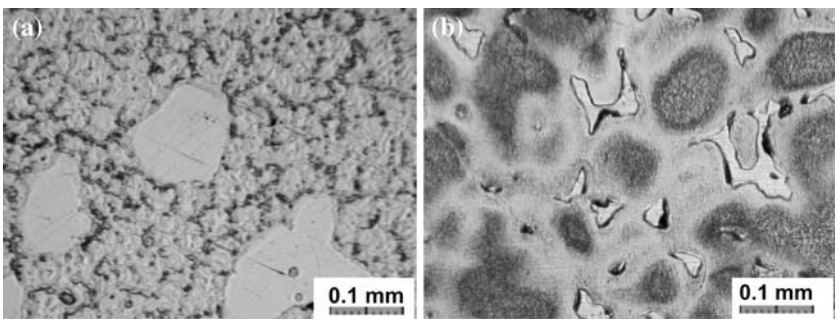

Fig. 1 (**a**) Microstructure of thixomolded AZ91 base material, (**b**) Microstructure of as-cast AZ91D base material

coupled to a data acquisition system. The key parameters (axial force, torque, rotational speed, pin displacement, shoulder, and pin temperature) were logged during all spot welding trials.

The tool shoulder and pin temperatures were measured by holding the pin stationary and rotating the Mg-alloy test sample. About 0.25 mm diameter K-type thermocouples were inserted into 1.0 mm diameter holes in the tool assembly, in such a way that the tips of the thermocouples were directly in contact with plasticized material during spot welding. The peak temperature was measured 0.2 mm from the base of the pin while the shoulder temperature was measured at a location 1.5 mm from the shoulder periphery. It has been shown elsewhere that the temperature measurement set-up produces results, which are ±6.4 °C about the mean value [3].

The temperature cycles in AZ91 material beneath the tool shoulder and parallel to the tool axis were measured by drilling holes and inserting thermocouples into the AZ91 sections prior to spot welding. This output provided information concerning the thermal cycle at these locations and the cooling rate following extraction of the rotating tool. About 0.25 mm diameter K-type thermocouples were located 1 mm below the upper surface of the AZ91 sheet at a distance of 2 mm from the pin periphery shoulder when measuring the thermal cycle in material beneath the tool shoulder. The thermocouples were located 0.4 mm from the periphery of the rotating pin prior to spot welding, level with the bottom of the keyhole when measuring the thermal cycle parallel to the tool axis.

The rotating tool cannot be withdrawn at the end of the spot welding operation without significantly deforming and displacing plasticized material immediately adjacent to the pin periphery. The incorporation of material into the stir zone was, therefore, investigated in trials where the spot welding operation was suddenly terminated so that the steel tool was 'frozen in place'. Detailed examination of material retained at the root of the pin thread was facilitated by carrying out the spot welding operation in a container holding a mixture of ethanol and liquid nitrogen at a temperature of –80 °C. A particularly high plunge rate (25 mm/s) was used during spot welding in combination with extremely short dwell periods to investigate how material from the locations beneath the tool shoulder and from the bottom of the rotating pin is incorporated into the stir zone. The rapidly-cooled spot welds were sectioned through the center of the steel tool using a diamond cutting wheel and all metallographic sections were etched in either 5 vol.% nital solution and/or acetic-picral solution comprising 10 mL acetic acid, 4.2 g picric acid, 10 mL H_2O and 70 mL of 95% ethanol.

The incorporation of material during the dwell period in AZ91 spot welding was examined by introducing alumina (Al_2O_3) tracer material into the stir zone. Alumina tracer material was introduced using the following procedure. The rotating pin was fully penetrated into the AZ91 sheet and was then withdrawn. Care was taken to make sure that the tool shoulder only just contacted the upper sheet surface during tool penetration. Sixteen 0.4 mm diameter × 1 mm deep holes were then drilled around the circumference of the keyhole at the radial location 0.5 mm from the keyhole periphery and were filled with alumina powder. The spot welding operation was then repeated using identical welding parameter settings with the addition of a 4-s long-dwell period. Tool rotation was suddenly terminated at the end of the spot welding operation and both the steel tool and the stir zone were sectioned during the preparation of metallographic samples. Although this incorporation technique proved successful, it is important to point out that only limited amounts of the alumina tracer material were introduced into the stir zone. For this reason, the identification of alumina tracer particles was carried out using a combination of optical and SEM microscopy.

Results

Figure 3a and b show the temperature output produced during friction stir spot welding of thixomolded AZ91 and as-cast AZ91D using a tool rotational speed of 3,000 rpm and plunge rates of 2.5 and 5.0 mm/s. It is readily apparent that the measured temperature varies during the dwell period in spot welding. In Fig. 3a, for example, the temperature decreases from 453 to 438 °C midway through the dwell period in spot welding. A temperature of 453 °C corresponds with $0.98T_s$, where T_s is the solidus temperature of AZ91 (in degree Kelvin) while 438 °C is close to the α-Mg + $Mg_{17}Al_{12}$ eutectic temperature (437 °C) in the Al–Mg binary equilibrium phase diagram. Also, the shoulder temperature rises to 421 °C at the end of the 4-s dwell period; this temperature corresponds with the reported temperature for burning during high temperature deformation of AZ91 sections, see Fig. 3a [14]. Lower temperatures were measured by the thermocouple contained within the tool shoulder since all AZ91 spot welding operations were terminated when the rotating pin was fully-penetrated and tool shoulder just contacted the upper sheet surface.

In Fig. 3b, the highest temperature during the dwell period in as-cast AZ91D spot welding fluctuates above and below 437 °C early in the dwell period. The temperature then rises to 454 °C toward the end of the dwell period. In contrast, the tool shoulder temperature levels off briefly at 421 °C at the start of the dwell period and then rises to 433 °C. Similar peak temperature output to that shown in Fig. 3a and b was produced during repeat testing of thixomolded and as-cast AZ91 test samples.

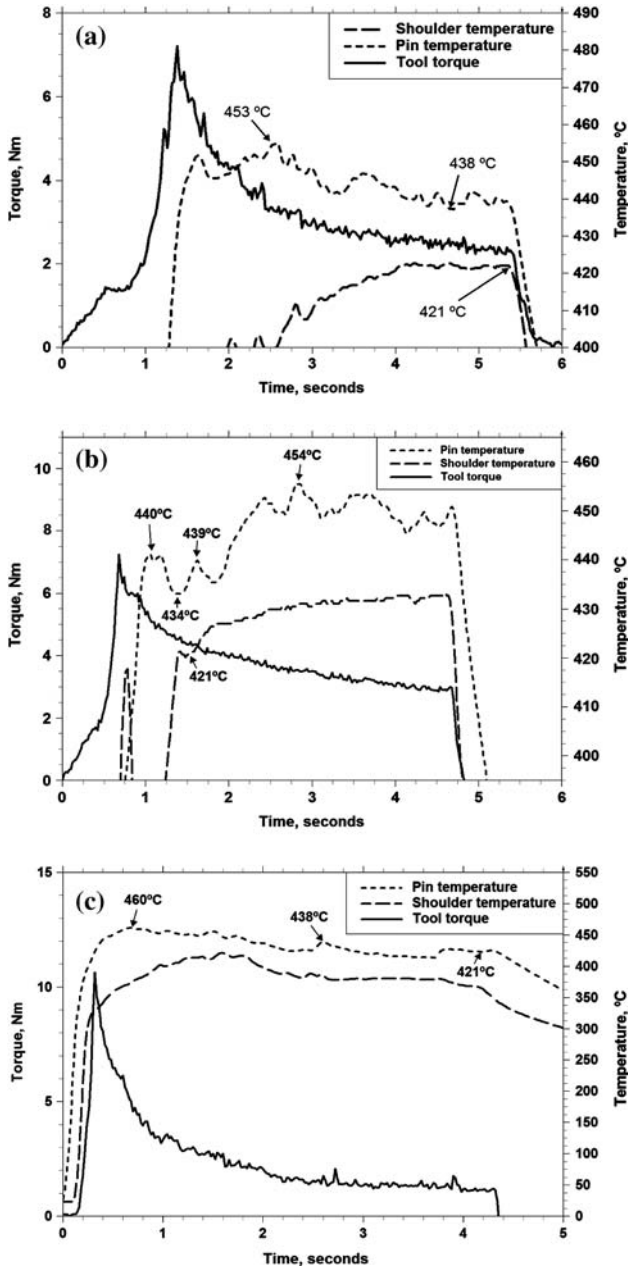

Fig. 3 (**a**) Temperature and torque output during spot welding of thixomolded AZ91 material using a tool rotational speed of 3,000 rpm and a plunge rate of 2.5 mm/s. (**b**) Temperature and torque output during spot welding of as-cast AZ91D material using a tool rotational speed of 3,000 rpm and a plunge rate of 5.0 mm/s. (**c**) Temperature and torque output during spot welding of thixomolded AZ91 using a tool rotational speed of 3,000 rpm, a plunge rate of 25 mm/s and a dwell time of 4 s

Figure 3c shows the temperature cycle produced during spot welding of thixomolded AZ91 material using an extremely rapid plunge rate (25 mm/s). The temperature rises extremely rapidly (around 1,800 °C/s) close to the tip of the rotating pin during the tool penetration stage in spot welding (in the period from 0 to 0.2 s). The temperature at the location 200 μm from the tip of the rotating pin is around 437 °C within 0.4 s of process initiation and subsequently increases to 460 °C before decreasing to 438 °C and then to 421 °C at the end of the spot welding operation.

Figure 4a shows the thermal cycle when a thermocouple is located 1 mm below the upper surface of the AZ91 sheet and at a distance of 2 mm from the pin periphery. The highest temperature in this location is much less than that measured using the thermocouple, which is located within the tool itself. It is also apparent that heat generation during the tool penetration stage in spot welding raises the temperature at the thermocouple location prior to contact between the bottom of the tool shoulder and upper sheet surface.

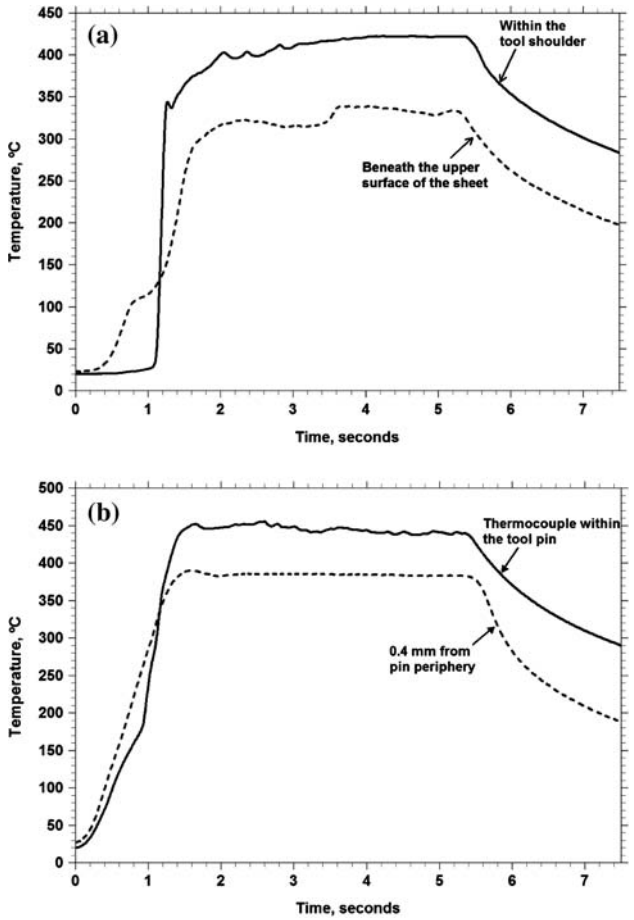

Fig. 4 (**a**) Temperature output measured by a thermocouple located 1 mm beneath the upper surface of AZ91 sheet and 2 mm from the pin periphery prior to spot welding and the tool shoulder temperature measured by the thermocouple located within the tool itself. During spot welding of thixomolded AZ91 using a tool rotational speed of 3,000 rpm, a plunge rate of 2.5 mm/s and a dwell time of four seconds. (**b**) Temperature output measured when a thermocouple is located 0.4 mm from the periphery of the rotating pin prior to spot welding and the temperature is measured by the thermocouple located within the tool itself the pin itself (at the location 0.2 mm from its tip). During spot welding of thixomolded AZ91 using a tool rotational speed of 3,000 rpm, a plunge rate of 2.5 mm/s and a dwell time of 4 s

Figure 4b shows the thermal cycle measured when thermocouples were placed 0.4 mm from the periphery of the rotating pin prior to AZ91 friction stir spot welding. The temperature increases at about 275 °C/s to a maximum temperature of around 390 °C, a value, which is much less than that measured using the thermocouple, which was located within the tool itself; see Fig. 4b. Following tool retraction, the spot weld cools from 380 to 200 °C in a period of 1.7 s.

Figure 5 shows metallographic evidence confirming local melted film formation within the stir zone of an AZ91 spot welded joint made using a plunge rate of 2.5 mm/s and a dwell time of 0.25 s.

Figure 6 shows the microstructural features of material located at the root of the pin thread in AZ91 spot welds produced using a very rapid plunge rate (25 mm/s) and dwell times of 0.25 and 0.75 s. The aluminum content of material at the root of the pin thread is much higher than that in the bulk of the stir zone, see locations A, B and C in Fig. 6(c). The chemical composition of material at the root of the pin thread is similar to that found when examining (α-Mg + $Mg_{17}Al_{12}$) eutectic formed in dissimilar Al 6111/AZ91 friction stir spot welds [5] and in Al 5754 spot welds made using a tool contaminated with magnesium prior to welding [7].

The movement of material downwards via the pin thread and into the stir zone during the dwell period in AZ91 spot welding was investigated by examining the movement of alumina tracer particles. Figure 7b shows alumina tracer

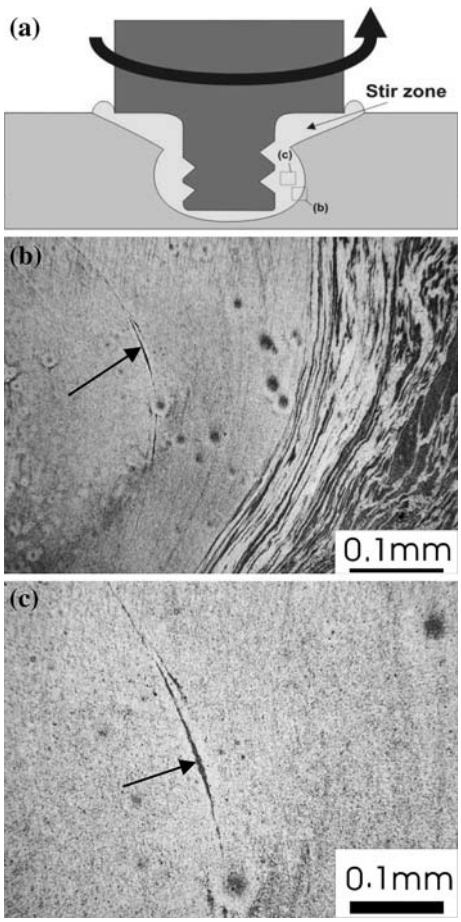

Fig. 5 (**a**) Schematic of friction stir spot weld and tool during spot welding, showing locations of local melted films observed in the stir zone. (**b**) and (**c**) Optical micrographs showing local melted films formed in the stir zone of a quenched AZ91 spot weld made using a plunge rate of 2.5 mm/s and a dwell time of 0.25 s (see arrows)

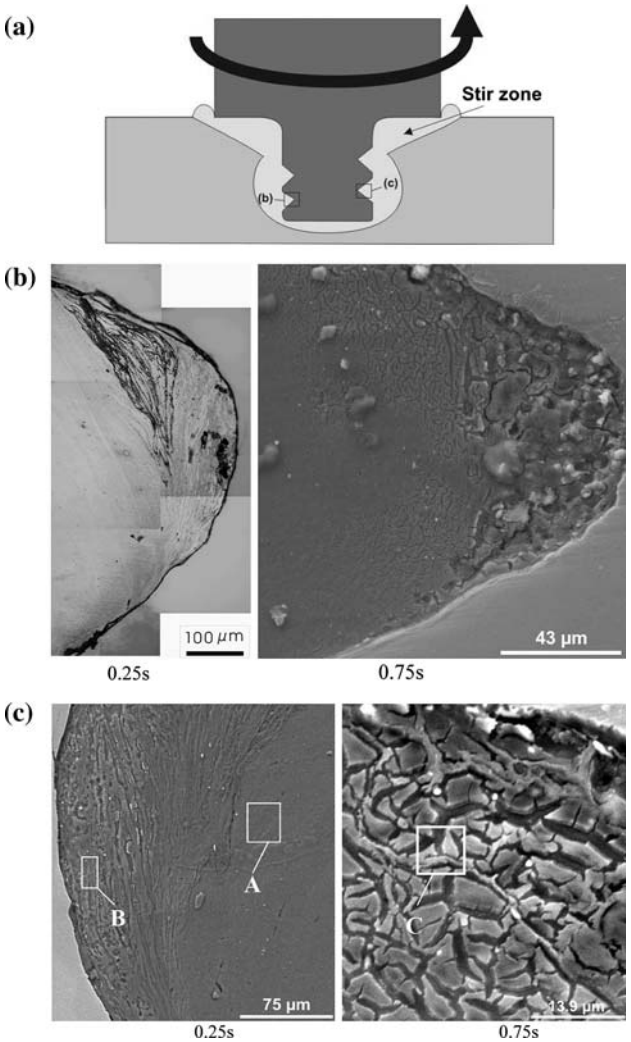

Fig. 6 (**a**) Schematic of friction stir spot weld and tool during spot welding, showing locations examined at the root of the pin thread in Fig. 6b and c. (**b**) Material at the root of the pin thread in rapidly-quenched AZ91 spot welds made using a plunge rate of 25 mm/s, a tool rotational speed of 3,000 rpm showing the microstructure (in a 0.25 s dwell time spot weld) and an SEM micrograph (in a 0.75 s dwell time spot weld). (**c**) SEM micrographs showing material located at the root of the pin thread in rapidly-quenched AZ91 spot welds made using dwell times of 0.25 and 0.75 s. The chemical composition at each location is: Element wt% Mg, Location A—83.3, Location B—80.9, Location c—79.8; Element wt% Al, Location A—11.7, Location B—19.1, Location c—20.2

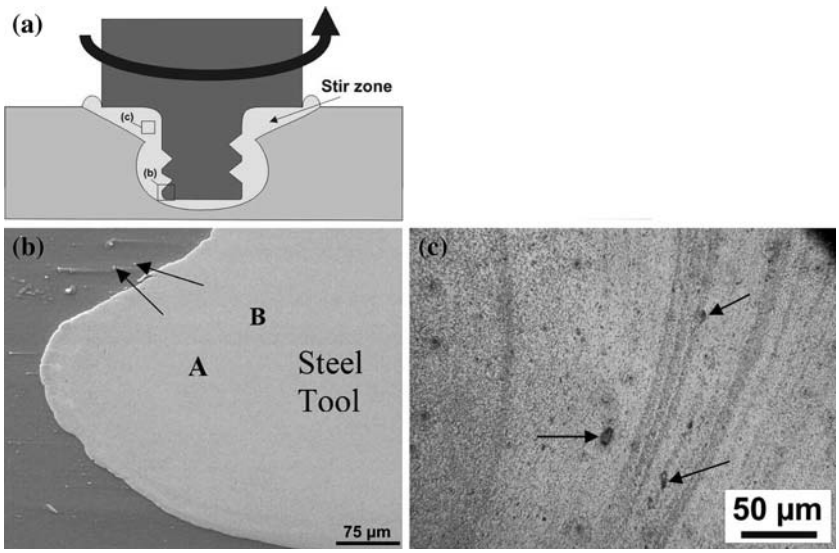

Fig. 7 (**a**) Schematic of friction stir spot weld and tool during welding, showing locations of alumina tracer particles in Fig. 7b and (c). (**b**) SEM micrograph showing alumina tracer particles at the root of the pin thread. (**c**) Micrograph showing alumina tracer particles within the stir zone. The particles were moved downwards via the pin thread during the dwell period in AZ91 spot welding, see A and B. In a spot weld made using a dwell time of 4 seconds, a tool rotational speed of 3,000 rpm and a plunge rate of 2.5 mm/s

particles moved downwards during the dwell period in spot welding and retained at the root of the pin thread while Fig. 7c shows alumina tracer particles contained within the stir zone of a completed spot weld.

Discussion

Temperature output

Since the microstructures of the as-cast AZ91D and thixo-molded AZ91 sections comprise a mixture of α-Mg and (α-Mg + $Mg_{17}Al_{12}$) eutectic the location where each spot weld is made will determine the peak temperature, which is measured at the start of the dwell period in sport welding. When the location where the rotating pin penetrates during spot welding is rich in α-Mg nodules the temperature at the start of the dwell period increases to about 453 °C and this corresponds with $0.98T_s$, where T_s is the solidus temperature of AZ91 base material in degrees Kelvin, see Fig. 3a. However, when the spot weld is made in a location, which is rich in (α-Mg + $Mg_{17}Al_{12}$) eutectic the temperature close to the tip of the rotating pin will increase rapidly to around 437 °C, which corresponds with the eutectic temperature in the binary Al–Mg equilibrium phase diagram, see Fig. 3b.

Figure 3a and b show that the temperature measured at the location within 200 μ m of the tip of the rotating pin varies during the dwell period in AZ91 spot welding. When the temperature at the start of the dwell period is around 437 °C the incorporation of material rich in α-Mg from the locations beneath the tool shoulder and the bottom of the rotating pin will increase the temperature to around 453 °C. In contrast, the incorporation of material rich in (α-Mg + $Mg_{17}Al_{12}$) eutectic will lower the temperature from 453 °C to around 437 °C, see Fig. 3a and b.

The heating rate during the pin penetration stage in AZ91 spot welding increases markedly when higher plunge rates are applied. For example, the heating rate increases from around 270 to 1,800 °C/s when the plunge rate increases from 2.5 to 25 mm/s during spot welding using a tool rotational speed of 3,000 rpm. During spot welding using a plunge rate of 25 mm/s the temperature reaches about 437 °C within 0.4 s of process initiation and then continues to increase to 460 °C (or $0.99T_s$), see Fig. 3c. The results shown in Fig. 3c provide strong experimental support for the proposal made by Bendzsak [15] and North [16] that the peak temperature during friction stir welding will approach the solidus temperature of the sheet material being welded.

Figure 4a shows the temperature cycle measured when a thermocouple is located 1 mm below the upper surface of the AZ91 sheet and at a distance of 2 mm from the periphery of the rotating pin prior to friction stir spot welding. In a similar manner, Fig. 4b shows the temperature cycle measured when a thermocouple is located at a distance of 0.4 mm from the periphery of the rotating pin prior to friction stir spot welding. In both cases metallographic examination confirmed that the thermocouples measured the thermal cycle in the thermo-mechanically affected zone (TMAZ) adjacent to the stir zone. This explains the large difference between the measured peak temperatures and those measured using thermocouples, which are located within the tool itself. It is well-documented that temperature decreases markedly at small distances from a contact surface, which is frictionally heated [17, 18]. It is particularly interesting that the temperature cycle within the stir zone was not measured when thermocouples were placed at a distance of 0.4 mm from the periphery of the rotating pin prior to spot welding. In the present study, the drilled holes containing the K-type

thermocouples are displaced both laterally and downwards during the friction stir spot welding operation and the thermal cycle in the TMAZ region, not the stir zone, is measured. These experimental results highlight the difficulties, which are encountered when the temperature during friction stir spot welding is measured using thermocouples, which are not located within the tool itself. Also, this may explain why there is considerable scatter in measured temperature values when the temperature during friction stir seam welding is measured by locating thermocouples ahead of the traversing tool. For example, Song et al. [19] reported temperature values ranging from 515 to 565 °C during seam welding of Al 6061-T6 while Colegrove et al. [20] measured temperatures ranging from 520 to 550 °C during seam welding of Al 7075-T7351.

Material incorporation

The dimensions of the stir zone formed adjacent to the periphery of the rotating pin are markedly increased during the dwell period in spot welding since material from the locations beneath the tool shoulder and the bottom of the rotating pin is incorporated at the top of the thread on the rotating pin and is moved downwards via the pin thread and into the stir zone [9, 10]. Figures 6 and 7 show the downward movement of material via the pin thread during the dwell period in AZ91 spot welding. The microstructure and chemical composition of material found at the root of the pin thread is quite different from that in the bulk of the stir zone in AZ91 spot welds produced using a plunge rate of 25 mm/s and dwell times of 0.25 and 0.75 s. Figure 7 shows that alumina tracer particles are transferred downwards via the pin thread during the dwell period in AZ91 spot welding.

The stir zone produced during AZ91 spot welding comprises intermingled lamellae, see Fig. 8. It has been recently suggested that the intermingled lamellae are formed when material from beneath the tool shoulder and the bottom of the rotating pin is incorporated at the top of the thread on the rotating pin and is transferred downwards via the pin thread [10]. The resulting ribbon of contiguous lamellae is discharged from the bottom of the thread on rotating pin and moves outwards and upwards following a helical vertical rotational flow path, see Fig. 9. When the material returns to the bottom of the rotating pin once again, the helical vertical rotational flow path is repeated, but further out from the pin periphery. A steady-state situation is attained and the width and height of the stir zone reach constant values. When this occurs, all of the material within the stir zone follows the same helical vertical rotational flow path. It is readily apparent that there is remarkable similarity between the numerical modeling

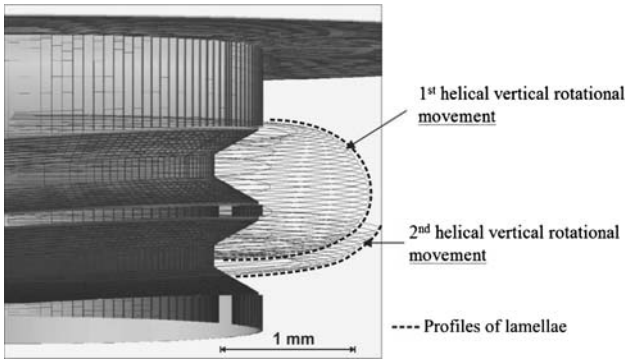

Fig. 9 Numerical modeling output showing the development of a helical vertical rotational flow during the dwell period in spot welding (after Ref. [10])

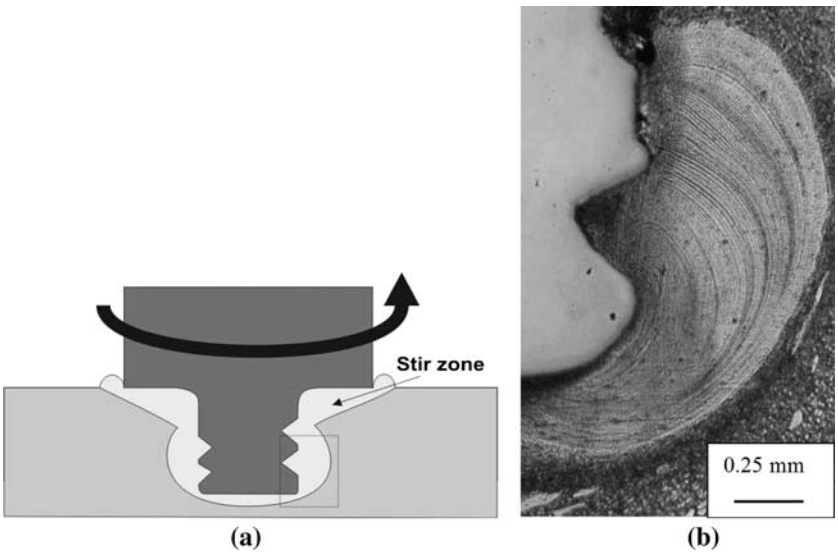

Fig. 8 (**a**) Schematic of friction stir spot weld and tool during welding, showing location of intermingled lamellae in the stir zone. (**b**) Intermingled lamellae in the stir zone of an AZ91 spot weld made using a dwell time of 4 s, a tool rotational speed of 3,000 rpm and a plunge rate of 2.5 mm/s

output shown in Fig. 9 and the microstructure of the stir zone produced during AZ91 spot welding, see Fig. 8.

The microstructure of as-cast AZ91D material comprises cored α-Mg with a divorced (α-Mg + $Mg_{17}Al_{12}$) eutectic located at interdendritic boundaries. Similarly, the microstructure of thixomolded AZ91 comprises α-Mg nodules contained in matrix of α-Mg and (α-Mg + $Mg_{17}Al_{12}$) eutectic, see Fig. 1a and b. The thermomechanical cycle during the tool penetration stage in friction stir spot welding elongates α-Mg grains and fragments $Mg_{17}Al_{12}$ particles, which begin to dissolve in the TMAZ region. Figure 10b and c show the microstructural features of the TMAZ immediately adjacent to the stir zone extremity at the locations halfway up the rotating pin and close to the top of the thread on the rotating pin.

The microstructure and chemical composition of material observed located at the root of the pin thread and the temperature cycle in AZ91 spot welds produced using a plunge rate of 25 mm/s and dwell times of 0.25 and 0.75 s are consistent with the proposal that eutectic melting occurs as material is transferred downwards via the pin thread, see Figs. 3c, 6b and c. Figure 3c shows that the temperature in the stir zone at the start of the dwell period in AZ91 spot welding is close to the eutectic temperature (437 °C). When melted eutectic is discharged from the bottom of the thread on the rotating pin it will follow a helical vertical rotational flow path within the stir zone, see Figs. 8 and 9. This may account for the curved profile of the local melted film shown in Fig. 5b and c.

Dissolution of liquid droplets in completed spot welds

Eutectic material will melt when it is incorporated into the stir zone during the dwell period in AZ91 spot welding. Once formed, the liquid droplets will begin to dissolve. Using Whelan's methodology [21], the dissolution of spherical liquid droplets is determined by the relation:

$$\left(\frac{R}{R_0}\right)^2 = 1 - t\left(\frac{a}{R_0}\right)^2$$

where R_0 is the initial radius, t is time and a is a constant that depends on the driving force for solute diffusion. The dissolution time can be calculated using the relation:

$$t = \left(\frac{R_0}{a}\right)^2$$

When plate-shaped droplets are considered:

$$B = B_0 - \frac{k}{\sqrt{\pi}}\sqrt{Dt}$$

where B is the droplet thickness, B_0 is the initial droplet thickness, D is the solute diffusion coefficient and k is the thermodynamic driving force for the dissolution process.

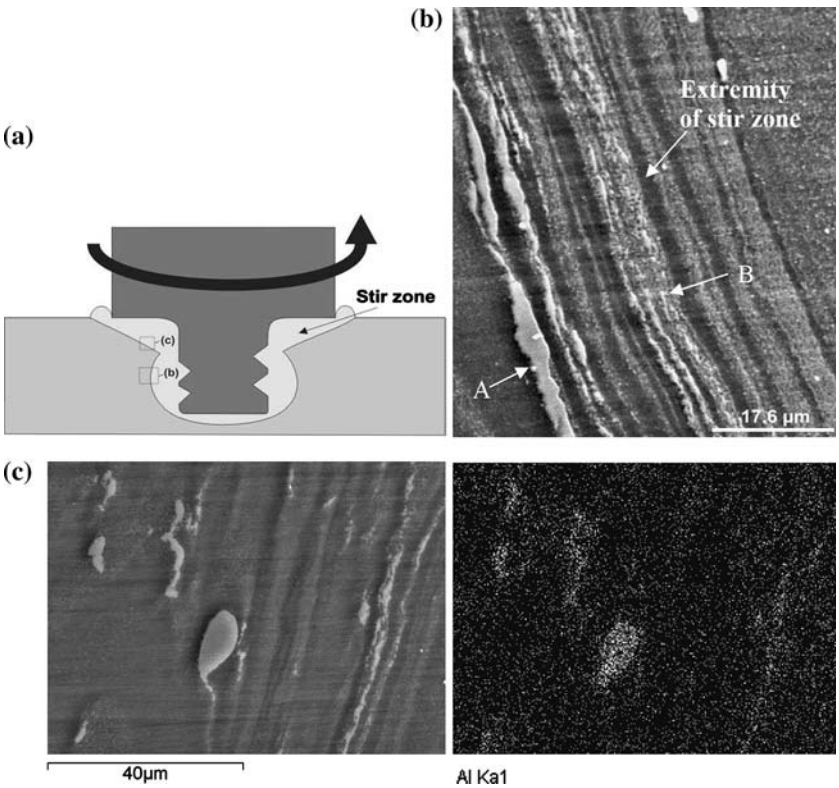

Fig. 10 (**a**) Schematic of friction stir spot weld and tool during welding, showing locations in the TMAZ region indicated in (**b**) and (**c**) below. (**b**) Fragmentation and dissolution of $Mg_{17}Al_{12}$ particles in the TMAZ region immediately adjacent to the stir zone extremity (see arrows A and B). At the location corresponding with halfway up the rotating pin in an AZ91D spot welding made using a dwell time of 4 s, a tool rotational speed of 3,000 rpm and a plunge rate of 2.5 mm/s (**c**) SEM image and EDX map of $Mg_{17}Al_{12}$ particles in the TMAZ region immediately adjacent to the stir zone extremity at the location close to the top of the thread on the rotating pin in an AZ91D spot welding made using a dwell time of 4 seconds, a tool rotational speed of 3,000 rpm and a plunge rate of 2.5 mm/s

The dissolution of liquid droplets during AZ91 spot welding is determined by the following factors:

a) The melting temperature; 437 °C during AZ91 spot welding
b) The diffusion coefficient of solute atoms at 437 °C; $D_{\text{Al in Mg}}$ is 9.73×10^{-3} μm^2/s and $D_{\text{Mg in Mg}}$ is 1.35×10^{-2} μm^2/s at 437 °C
c) The thermodynamic driving force for dissolution; k = 0.4, see the Appendix
d) The shape and dimensions of the liquid droplets
e) The time available for dissolution during the dwell period in spot welding
f) Particle dissolution when the spot weld cools to room temperature

Figure 11 shows the relation between the liquid droplet dimensions and the time available for dissolution at a temperature of 437 °C. It is worth noting that the formation of spherical liquid droplets is more likely since fragmentation of elongated, rod-like intermetallic and alumina particles has been confirmed during friction stir welding [22, 23] and the surface energy per unit volume is minimized when spherical droplets are formed. A 0.25 μm diameter spherical droplet will be completely dissolved in 4 s, see Fig. 11. However, since material from beneath the tool shoulder and the bottom of the rotating pin is incorporated throughout the dwell period in spot welding the time available for dissolution of liquid droplets will be determined when the melting event occurs. Consequently, the time available for dissolution in Fig. 11 does not correspond with the dwell time employed during AZ91 spot welding. In addition, when liquid droplets are not completely dissolved at the end of the dwell period and solidification occurs, particle dissolution will continue as the AZ91 spot weld cool to room temperature. The dissolution tendency of spherical particles when AZ91 spot welds cool to room temperature is indicated in Fig. 12. A detailed description of the calculation method is provided in the Appendix.

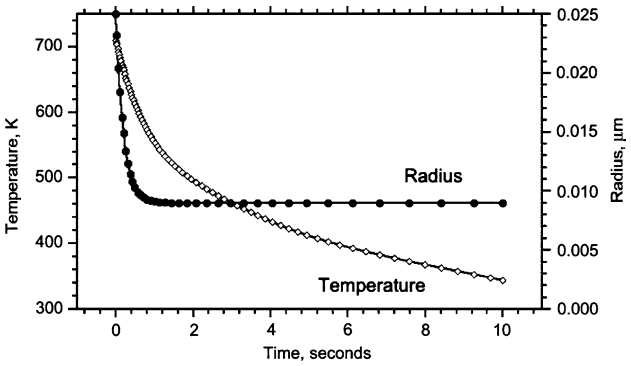

Fig. 12 Dissolution of spherical particles when the AZ91 spot weld cools in air following tool extraction

Figure 5 shows evidence of local melted film formation in an AZ91 spot weld produced using a plunge rate of 2.5 mm/s and a dwell time of 0.25 s. The likelihood of finding metallographic evidence confirming local melted film formation during friction stir spot welding will markedly depend on the eutectic melting temperature, the dissolution kinetics at that temperature and the liquid droplet shape and dimensions. For example, it has recently been suggested that tool slippage during Al 7075-T6 spot welding results from melting of second-phase η particles when the welding parameter settings produce stir zone temperatures ≥ 475 °C [3]. The solute diffusion rate is much higher ($D_{\text{Zn in Al}} = 1.23 \times 10^{-1}$ μm^2/s) and the thermodynamic driving force for droplet dissolution is also much larger (k = 1.46) when melted eutectic droplets are formed at 475 °C. As a result, it would be expected that melted eutectic droplets would dissolve much faster during the dwell period in Al 7075-T6 spot welding than they would during the dwell period in AZ91 spot welding, see

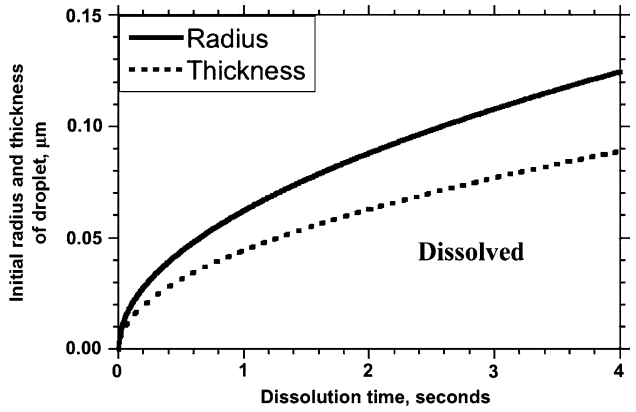

Fig. 11 Relation between the dissolution time and the dimensions of spherical and plate-shaped liquid droplets formed in the stir zone during AZ91 spot welding

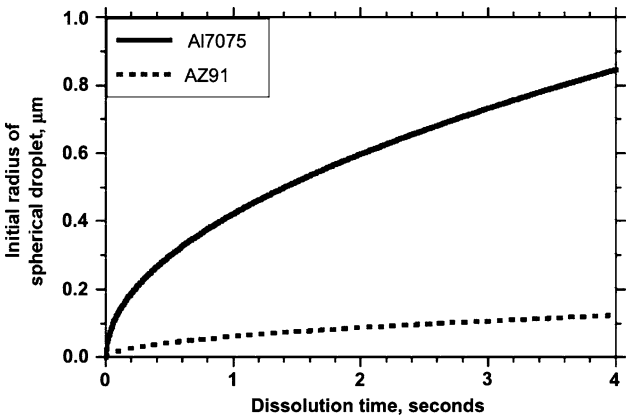

Fig. 13 Comparison of the dissolution kinetics of spherical liquid droplets formed in the stir zones of Al 7075-T6 and AZ91 spot welds

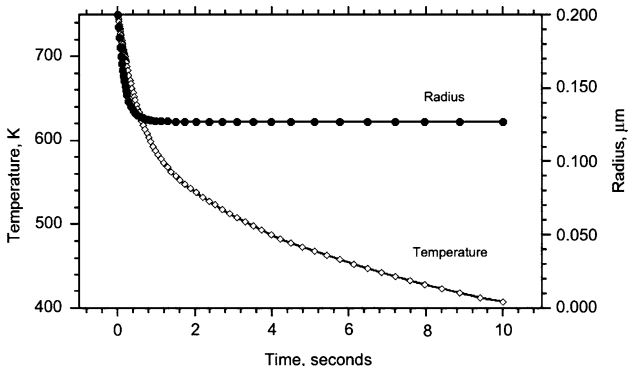

Fig. 14 Dissolution of spherical particles when the Al 7075-T6 spot weld cools following tool extraction

Fig. 13. If 0.1 μm diameter spherical melted droplets are formed in the stir zone during Al 7075-T6 friction stir spot welding, they will be completely dissolved unless they are produced very late in the dwell period. In this connection, Fig. 14 indicates that 0.1 μm particles will dissolve as the Al 7075-T6 spot weld cools to room temperature following tool retraction. This may well explain why unequivocal metallographic evidence supporting the melted eutectic film formation in Al 7075-T6 friction stir spot welds is difficult to find.

Conclusions

A detailed investigation of friction stir spot welding of as-cast AZ91D and thixomolded AZ91 of sections has confirmed that:

1. The average temperatures measured close to the tip of the rotating pin vary from 438 to 454 °C during the dwell period in AZ91D spot welding depending on relative proportions of α-Mg and (α-Mg + $Mg_{17}Al_{12}$) eutectic, which are incorporated into the stir zone. A temperature of 454 °C corresponds with $0.98T_s$, where T_s is the solidus temperature of AZ91 in degrees Kelvin while 438 °C is very close to the α-Mg plus (α-Mg + $Mg_{17}Al_{12}$) eutectic temperature in the Al–Mg binary equilibrium phase diagram. Also, the peak temperature (460 °C) measured close to the tip of the rotating pin in AZ91 spot welds made using a particularly high plunge rate (25 mm/s) corresponds with $0.99T_s$.
2. Eutectic melting occurs as material is transferred downwards via the pin thread during the dwell period in spot welding based on a detailed examination of (i) the temperature cycle in rapidly-quenched AZ91 spot welds made using a plunge rate of 25 mm/s and dwell times of 0.25 and 0.75 s and (ii) the microstructure and chemical composition of material found at the root of the pin thread. Metallographic evidence confirming melted eutectic film formation was also found in the stir zones of AZ91 spot welds produced using a plunge rate of 2.5 mm/s and a dwell time of 0.25 s.
3. The factors determining the dissolution of melted droplets formed in the stir zones of AZ91 and Al 7075-T6 spot welds were compared. The likelihood of droplet dissolution is much greater during Al 7075-T6 spot welding since the melting temperature (475 °C c.f. 437 °C), the solute diffusion rate and the thermodynamic driving force for droplet dissolution are much higher. This may explain why metallographic evidence supporting the melted eutectic film formation is found in AZ91 friction stir spot welds and is not found in Al 7075-T6 friction stir spot welds.

Acknowledgements The authors wish to acknowledge financial support from the Natural Sciences and Engineering Research Council of Canada during this project.

Appendix

Dissolution of liquid droplets in an AZ91 stir zone

The Fig. A1 shows part of the binary Mg–Al equilibrium phase diagram:

The driving force for diffusion and dissolution of liquid droplets is determined by the relation:

$$k = 2\left[\frac{C_{T_2}^{\alpha/\mathrm{liq}} - C_{T_1}^{\alpha/\beta}}{C_{T_2}^{\mathrm{liq}/\alpha} - C_{T_2}^{\alpha/\mathrm{liq}}}\right]$$

For AZ91; k = 0.4, $C_{T_1}^{\alpha/\beta} = 9\%$, $C_{T_2}^{\alpha/\mathrm{liq}} = 13\%$, $C_{T_2}^{\mathrm{liq}/\alpha} = 33\%$, $T_2 = 710\,\mathrm{K}$.

The diffusion coefficient depends on the relation:

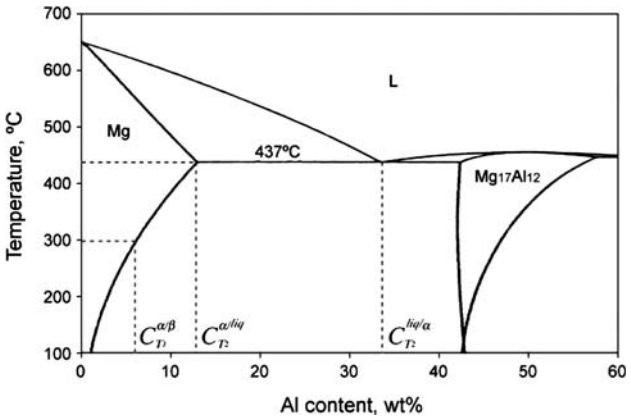

Fig. A1 Mg-rich portion of the binary Mg–Al equilibrium phase diagram

$$D = D_0 \exp\left[-\frac{Q}{RT}\right]$$

where,

$R = 8.314 \times 10^{-3}$ kJ/(mol · K)

and the diffusion rate of Al in Mg is [1A]: $D_{\text{Al in Mg at 710 K}} = 3.89 \times 10^{-3}$ μm^2/s at 710 K

$D_0 = 1.53 \times 10^7$ μm^2/s, $Q = 125$ kJ/mol.

The relation between the half-thickness of a plate-shaped liquid droplet or the radius of a spherical droplet and the time available for dissolution at 710 K is determined by the relation:

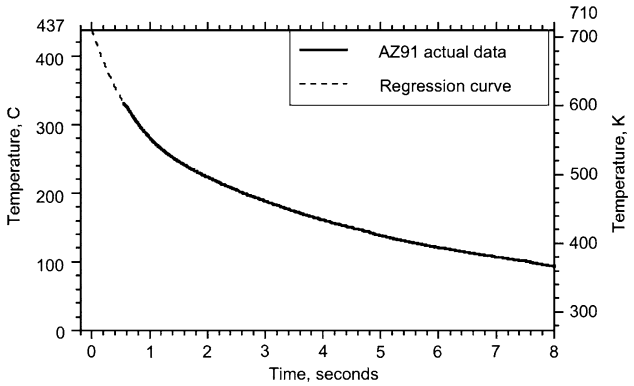

Fig. A2 Thermal cycle during cooling period following AZ91 spot welding

$$B_0 = \frac{k}{\sqrt{\pi}}\sqrt{D_{\text{Al in Mg at 710 K}} \cdot t}, \quad R_0 = \sqrt{k \cdot D_{\text{Al in Mg at 710 K}} \cdot t}$$

Dissolution when the spot weld cools to room temperature

Figure A2 shows the thermal cycle when the AZ91 spot weld cools to room temperature. A 7th power polynomial regression analysis was used to extrapolate the temperature output of AZ91 to that conforming to the stir zone temperature (437 °C (710 K)).

The calculation method employed during the cooling period following spot welding is illustrated in Fig. A3.

The cooling curve obtained from the regression was divided into about 10 °C increments and the diffusion rate (D_n) at each temperature (T_n) was obtained. The mass loss by particles in the stir zone during cooling was calculated during each time increment, see the above figure.

The diffusion thickness and radius were obtained by taking account of the previous interval effect. For example, during the ith time interval (from t_{is} to t_{ie}) the diffused thickness and radius are calculated using D_i:

For a plate-shaped droplet;

$$t_{\text{is}} = \frac{\pi B_{i-1}^2}{k^2 D_i}, \quad \Delta B_i = \frac{k}{\sqrt{\pi}}\left(\sqrt{D_i t_{\text{ie}}} - \sqrt{D_i t_{\text{is}}}\right),$$
$$B_i = B_{i-1} + \Delta B_i, \quad t_i = t_{i-1} + (t_{\text{ie}} - t_{\text{is}})$$

For a spherical droplet;

$$t_{\text{is}} = \frac{R_0^2 - R_{i-1}^2}{kD_i}, \quad R_i = R_0\sqrt{1 - \frac{kD_i}{R_0^2}t_{\text{ie}}}, \quad t_i = t_{i-1} + (t_{\text{ie}} - t_{\text{is}})$$

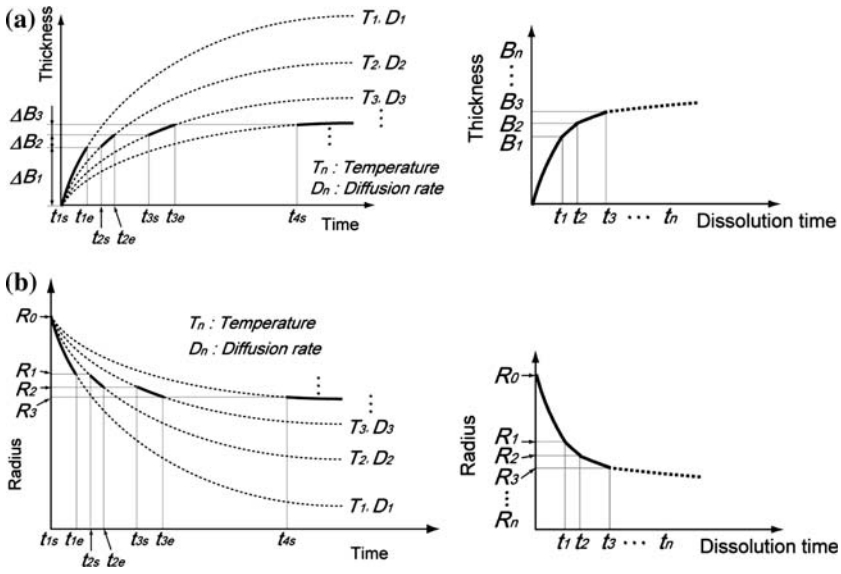

Fig. A3 Schematic illustration of the calculation method used when determining the non-isothermal dissolution rate of (**a**) plate-shaped and (**b**) Spherical droplets

The total diffused thickness (B_n) and the radius after cooling (R_n) during cooling was calculated during the final nth time interval.

Droplet dissolution in an Al 7075 stir zone

Figure A4 shows the pseudo binary Al-$MgZn_2$ phase diagram [2A] corresponding with Al 7075 alloy.

The driving force for diffusion and dissolution of liquid droplets of Al7075 is: k = 1.46, $C_{T_1}^{\alpha/\beta} = 7.5\%$, $C_{T_2}^{\alpha/\mathrm{liq}} = 17\%, C_{T_2}^{\mathrm{liq}/\alpha} = 30\%, T_2 = 748$ K and the diffusion rate of Zn in Al is [3A]: $D_{\mathrm{Zn\ in\ Al\ at\ 748\ K}} = 1.23 \times 10^{-1}\ \mu\mathrm{m}^2/\mathrm{s}$ at 748 K

$$D_0 = 1.05 \times 10^8\ \mu\mathrm{m}^2/\mathrm{s}, \quad Q = 128\ \mathrm{kJ/mol}$$

The relation between the half-thickness of a plate-shaped liquid droplet or the radius of a spherical droplet and the time available for dissolution at 748 K is determined by using the same equation for AZ91 indicated previously.

A 9th power polynomial regression analysis was used to extrapolate the temperature output below the shoulder to that conforming with a stir zone temperature of 475 °C (748 K) for the Al 7075 calculation, see Fig. A5.

Particle dissolution when the Al 7075 spot weld cools to room temperature follows the same procedure to that indicated previously. The same thermal cycle during air-cooling to room temperature is assumed.

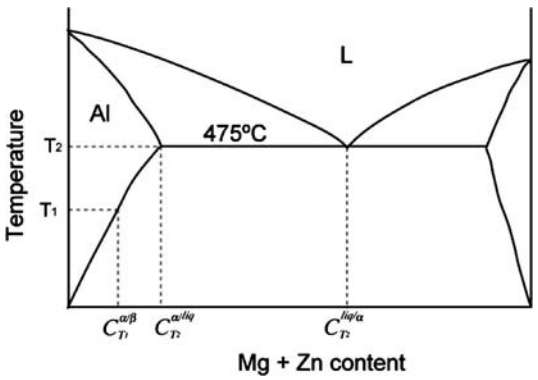

Fig. A4 Pseudo-binary Al–$MgZn_2$ equilibrium phase diagram

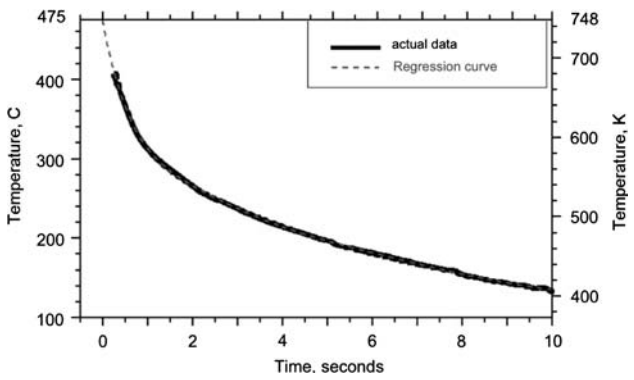

Fig. A5 Thermal cycle during cooling period following Al 7075 spot welding

Appendix references

1A. Japan Magnesium Association (2000) Handbook of advanced magnesium technology. p 132
2A. Hanemann H, Schrader A (1952) Ternäre Legierungen des Aluminiums. Verlag tahleisen M.B.H., Dusseldorf, p 138
3A. Bjørneklett B, Frigaard Ø, Grong Ø, Myhr OR, Midling OT (1998) Proc. 6th Internat. Conf. on Aluminium Alloys. Toyoashi, Japan, p 1531

References

1. Su P, Gerlich A, North TH, Bendzsak GJ (2006) Sci Tech Weld Joining 11(2):163
2. Su P, Gerlich A, North TH (2006) SAE Technical Series, 2006-01-0971
3. Gerlich A, Avramovic-Cingara G, North TH (2006) Metall Trans A 37A:2773
4. Gerlich A, Su P, North TH (2005) J Mat Sci 40:6473
5. Gerlich A, Su P, North TH (2005) Sci Tech Weld Joining 10(6):647
6. Gerlich A, Su P, North TH, Bendzsak GJ (2005) In: Nie JF et al (eds) Materials forum 29:290
7. Gerlich A, Su P, North TH (2005) In: Neelameggham NR, Kaplan HI, Powell BR (eds) Magnesium technology 2005. TMS, p 383
8. Lin P-C, Lin S-H, Pan J, Pan T, Nicholson JM, Garman MA (2004) SAE Technical Series, 2004-01-1330
9. Gerlich A, Su P, North TH, Bendzsak GJ (2006) Proc Friction Stir Welding Colloquium, Graz, Austria, May 23rd 2006
10. Su P, Gerlich A, North TH, Bendzsak GJ (2007) Metall Trans A 38A:584
11. Droenen P-E, Ryum N (1994) Metall Trans A 25A:521
12. Reiso O, Øverlie H-G, Ryum N (1990) Metall Trans A 21A:1689
13. Lohne O, Ryum N (1988) Proc. 4th Int. Aluminum extrusion technology seminar, Aluminum Association, vol II. 303
14. Lyman T (1961) ASM metals handbook, 8th edn. American Society for Metals, Metals Park, Ohio
15. Bendzsak GJ, North TH, Smith CB (2000) Proc. 2nd Int. Conf. Friction Stir Welding, Gothenburg, Sweden, TWI
16. North TH, Bendzsak GJ, Smith CB, Luan GH (2001) Proc. of the 7th Int. Symp. of JWS. p 621
17. Bowden FP, Ridler KEW (1936) Proc Roy Soc 154(883):640
18. Bowden P, Thomas PH (1954) Proc Roy Soc 223(1152):29
19. Song M, Kovacevic R (2002) Trans SME 621
20. Colegrove P, Shercliff H (2003) Sci Tech Weld Joining 8(5):360
21. Whelan MJ (1969) Met Sci J 3:95
22. Su J-Q, Nelson TW, Mishra M, Mahoney M (2003) Acta Mat 51:713
23. Su P, Gerlich A, North TH, Bendzsak GJ, (2006) Sci Tech Weld Joining 11(1):61